Article

Ruthenium Catalysts Supported on Hydrothermally Treated Carbon from Rice Husk: The Effect of Reduction Temperature on the Hydrogenation Reaction of Levulinic Acid to γ-Valerolactone

Virginia I. Rodríguez [ID], Gustavo Mendow, Bárbara S. Sánchez, Juan Rafael García *, Richard A. Pujro, Sergio R. de Miguel * and Natalia S. Veizaga

Instituto de Investigaciones en Catálisis y Petroquímica "Ing. José Miguel Parera" INCAPE (UNL–CONICET)
Colectora Ruta Nac. Nº 168 Km 0—Paraje El Pozo, Santa Fe 3000, Argentina; virodri@fiq.unl.edu.ar (V.I.R.);
gmendow@fiq.unl.edu.ar (G.M.); bsanchez@fiq.unl.edu.ar (B.S.S.); rpujro@fiq.unl.edu.ar (R.A.P.);
nveizaga@fiq.unl.edu.ar (N.S.V.)
* Correspondence: jgarcia@fiq.unl.edu.ar (J.R.G.); sdmiguel@fiq.unl.edu.ar (S.R.d.M.);
  Tel.: +54-(342)-451-1370 (ext. 6112) (J.R.G.)

Abstract: Ru catalysts supported on activated carbon obtained by hydrothermal treatment of rice husk were evaluated in the hydrogenation reaction of levulinic acid to γ-valerolactone. The hydrothermally treated carbon was characterized by nitrogen physisorption, elemental analysis, and thermogravimetric analysis, and the catalysts were characterized by FTIR spectroscopy, X-ray photoelectron spectroscopy, temperature-programmed reduction, and temperature-programmed desorption of pyridine (acidic properties). Prior to the reaction, the catalysts were reduced at different temperatures in the range of 100–350 °C to evaluate the effect of the reduction temperature on the performance in the hydrogenation of levulinic acid. The reaction was carried out in a batch reactor at 70 °C and 1.5 MPa. The results of conversion and selectivity to γ-valerolactone showed that the catalyst with the best performance was the sample reduced at 200 °C. After 2 h of reaction, a γ-valerolactone yield of 74% was achieved. This catalyst presented the lowest acidity value, and the ruthenium-containing phase consisted mainly of RuO_2, with a small portion of Ru^0. The solid catalyst can be recovered and successfully reused for three runs with the GVL yield at 56%.

Keywords: Ru catalyst; hydrothermally treated carbon; rice husk; levulinic acid hydrogenation; γ-valerolactone

1. Introduction

In today's era, the sustenance of economic growth depends on the availability of secure resources for industrial production, which must also have long-term availability. Unfortunately, fossil resources are not considered sustainable, and their long-term accessibility is even more uncertain. Given the reliance on finite petroleum resources and the growing environmental issues worldwide, biomass has become an attractive alternative source of feedstock for the production of bio-oil and synthesis gas. Despite this, a considerable amount of waste is produced during the process that can be harnessed as a source of low-value energy, either through incineration or disposal [1–4].

Activated carbon is a very useful carbonaceous material with a considerable surface area and a controllable pore structure. For these reasons, it is frequently employed in industry as an adsorbent to remove a variety of organic and inorganic contaminants from wastewater [5,6] and also as a catalyst support [7–9]. The preparation of high-yield activated carbon from biomass residues is promising. There are two preparation routes: physical and chemical. Among the most notable advantages of the chemical route, the low carbonization temperature, which would reduce energy consumption compared to a

physical process (which requires temperatures >900 °C), can be mentioned, and on the other hand, the activated carbon produced from chemical activation has a higher surface area and a well-developed porosity compared to that produced from physical activation [10]. It should be noted that the chemical route employs various activating agents such as $ZnCl_2$ [11,12], strong bases (NaOH or KOH) [13,14], and H_3PO_4 [12,14,15]. H_3PO_4 has attracted considerable attention as an activating agent due to its lower environmental and toxicological impact compared to $ZnCl_2$, as well as its lower operating temperature compared to KOH or NaOH [14]. In addition to the conventional method of producing activated carbons from agricultural byproducts, the hydrothermal carbonization process offers distinct advantages, as it can produce a diverse range of sustainable carbonaceous materials with desirable nanostructures and functionalization patterns suitable for various applications [16].

Levulinic acid (LA) is considered a crucial biomass platform molecule, owing to its ability to undergo chemical conversion into numerous secondary derivatives [17,18]. One of the most noteworthy uses of LA is its transformation into γ-valerolactone (GVL) through catalytic hydrogenation. This particular application has garnered significant interest due to the broad range of uses of GVL in the production of solvents and polymers, as well as, most notably, as a fuel additive [19–21]. Figure 1 shows a simplified scheme of the levulinic acid hydrogenation to produce γ-valerolactone.
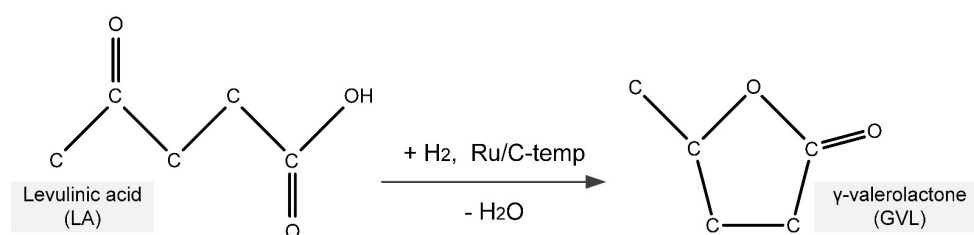

Figure 1. Simplified scheme of LA hydrogenation to GVL.

According to the literature, the hydrogenation of LA over a catalyst is the most efficient and economical method to produce GVL reported to date [22]. The first studies of LA hydrogenation date back to the first decades of the 20th century. Schutte et al. [23] reported the hydrogenation of LA in different organic solvents using a platinum oxide catalyst to produce 87% GVL yield after 44 h at a hydrogen pressure of 0.3 MPa. Christian et al. [24] reported a 94% GVL yield at 220 °C and 4.8 MPa using a Raney nickel catalyst in the liquid phase hydrogenation of LA. In addition, they used a copper chromite catalyst to hydrogenate LA at 273 °C and 10.1 MPa, and the yields of γ-valerolactone and 1,4-pentanediol were 62 and 21%, respectively.

Several heterogeneous catalysts have been studied during the last decades for this reaction. Usually, noble metals such as iridium (Ir) [25–27], palladium (Pd) [28–30], platinum (Pt) [31–33], and ruthenium (Ru) [34–48] are the most used catalysts. In particular, Ru catalysts are taken as reference catalysts for this reaction because high GVL yields (>97%) can be achieved [36]. It has been shown that supported Ru nanoparticles are active and selective catalysts due to their ability to activate the C=O bond in the LA and H_2 molecule [41–46]. However, the production of GVL might have a negative impact on the environment when compressed H_2 (3–4 MPa) and/or high reaction temperatures (≥140 °C) are used [42–44].

Concerning the supports, a variety of combinations have been used, such as silica, alumina, oxides, and carbon. Ru catalysts supported on mixed oxides Al_2O_3–TiO_2, Al_2O_3–MoO_3, and Al_2O_3–Co_3O_4 were studied in the conversion of levulinic acid to γ-valerolactone. NH_3-TPD results and catalytic behavior revealed that the Ru metal combined with strong acidic sites of support could promote the aqueous phase reforming, resulting in the lower yield of GVL [45]. In another study, a Ru/ZrO_2 catalyst could achieve 100% GVL yield at 150 °C and 3 MPa in dioxane [42]. Moreover, Cao et al. [44] synthesized a $Ru/ZrO_2@C$ catalyst that could provide a 96.4% GVL yield at 140 °C and 1 MPa in water. Although

carbon has been utilized as a catalyst support for many years, there has been a recent surge in research regarding the use of Ru supported on carbon for producing GVL. The liquid phase hydrogenation of LA with 5% Ru/C in a batch reactor was studied and 99% selectivity to GVL was obtained with 92% LA conversion at 130 °C and 1.2 MPa using methanol as solvent [40]. Liu et al. [47] developed a catalyst with uniform Ru nanoparticles incorporated into a mesoporous carbon support (Ru-MC). The support was synthesized using a SiO_2 template that was completely removed after calcination at 850 °C. The Ru-MC catalyst was used in the GVL production reaction with a constant pressure of 4 MPa. At 70 °C, 64% LA conversion and 63% GVL yield were obtained. Subsequently, the temperature was increased to 110 °C, obtaining 100% LA conversion and 99% GVL yield. Recently, a series of Ru/carbon nanosphere catalysts with tunable contents of interfacial C=O species were successfully synthesized, which were demonstrated to be highly efficient in the production of GVL under mild conditions (40 °C and 2 MPa) [48].

In this work, we developed Ru/carbon catalysts for the conversion of LA to GVL. On one hand, activated carbon was synthesized from biomass (rice husk) by means of hydrothermal treatment, capable of being used as a catalytic support. On the other hand, we investigated the optimal reduction temperature for Ru that leads to obtaining high LA conversion and GVL selectivity.

2. Materials and Methods

2.1. Catalyst Preparation

Rice husk from *Oryza sativa* L., with particle sizes in the range of 1.7–2.4 mm, was provided by a local mill from Santa Fe province (Santa Fe, Argentina).

2.1.1. Hydrothermal Treatment

For the preparation of hydrothermally treated carbon, the procedure described by Quesada et al. [16] was followed. The biomass (rice husk) was washed with tap water to remove impurities and then dried at 80 °C. Subsequently, 8.5 g of biomass was loaded into the autoclave reactor (total volume, 100 mL), and then 37 mL of phosphoric acid solution (23% *w/v*) was added before closing the reactor. The pressure in the system was autogenous. The temperature was maintained at 200 °C for 24 h. Once the time for the hydrothermal treatment was elapsed, the reactor was cooled down and opened. Then, the solid was filtered to separate the supernatant acid and air-dried for 48 h. After that, the carbonization stage was carried out under N_2 flow with a heating rate of 6 °C/min until 750 °C, where it was held for 2 h. Finally, the carbon was washed with 300 mL of distilled water at 65 °C in three stages (final pH value of 6.5). The nomenclature used for the hydrothermally treated carbon was HTC, while the virgin rice husk was called VRH.

2.1.2. Preparation of 2% Ru Supported Catalysts

The preparation of the catalysts with 2% Ru was carried out by the wet impregnation method, using HTC (hydrothermally treated carbon) as a support. During wet impregnation, the support was added to a Ru solution ($RuCl_3 \cdot 3H_2O$, Sigma Aldrich) under constant stirring, using a solution volume/support mass ratio of 30 mL/g. The suspension was stirred for 4 h and finally heated to evaporation at 120 °C to ensure complete metal deposition on the HTC. Subsequently, the reduction of the precursor was carried out in hydrogen flow at different temperatures for 2 h. The reduction temperatures used were 100, 150, 200, 275, and 350 °C. The nomenclature used to designate the different catalysts was as follows: Ru/C (unreduced sample), and Ru/C-100, Ru/C-150, Ru/C-200, Ru/C-275, and Ru/C-350, according to the reduction temperature.

2.2. Characterization

The properties of the rice husk and hydrothermally treated carbon were determined through ASTM D3173 (moisture content), ASTM D3175 (volatile matter), and ASTM D3174 (ash content) standards. Briefly, moisture was determined by establishing the sample loss

of weight when heated until 104–110 °C in a drying oven. Volatile matter was determined from the loss of weight after heating the sample at 950 °C in a platinum crucible closed with a cover that fits closely enough so that the carbon did not burn. Ash was determined by weighing the inorganic residue remaining after burning the sample at 750 °C in porcelain capsules. The fixed carbon content was calculated by difference. The composition of the ashes was determined by X-ray fluorescence spectrometry (EDX-720 model, Shimadzu). The elemental composition (CHON) was determined with the aid of a LECO CHN 628 Series Elemental analyzer [49].

The textural properties of virgin rice husk (VRH) and hydrothermally treated carbon (HTC) were determined by N_2 physisorption at −196 °C in Micromeritics ASAP 2020 equipment. Before the adsorption–desorption analysis, the samples were outgassed under vacuum (absolute pressure lower than 10^{-4} torr) at 130 °C for 8 h. The Brunauer–Emmet–Teller (BET) model was used in the 0.01 < P/Po < 0.03 range to calculate the BET-specific surface area. The total pore volume was calculated from the amount of nitrogen adsorbed until P/Po $\approx$ 0.98. The pore size distribution and the average mesopore diameter were determined with the aid of the Barrett–Joyner–Halenda (BJH) model, applied to the adsorption branch of the isotherms.

Thermogravimetric analyses (TGA) were performed in a Mettler Toledo TGA/SDTA851e thermobalance. Approximately 10 mg of sample was loaded into an alumina crucible and heated at 12 °C/min, from 20 °C to 900 °C with a N_2 flow rate of 50 mL/min.

The acidic properties were determined by means of temperature-programmed desorption (TPD) of pyridine (>99%, Cicarelli). Twenty milligrams of each solid were pretreated under N_2 flow (60 mL/min) at 500 °C for 1 h. After cooling to room temperature, the saturation with pyridine (Py) was carried out under N_2 stream (60 mL/min) with the aid of a saturator at 80 °C. Then, the temperature was increased to 150 °C and maintained at this temperature for 1 h with N_2 flow in order to remove the physically adsorbed pyridine. The TPD experiments were carried out by heating at 12 °C/min in the 150 to 700 °C range, the desorbed pyridine being submitted to methanation with a Ni catalyst and quantified with the aid of a flame ionization detector (FID) in a Shimadzu GC-8A gas chromatograph.

The ruthenium/activated carbon samples, both non-reduced precursor (Ru/C) and those that were reduced at different temperatures (Ru/C-100, Ru/C-150, Ru/C-200, Ru/C-275, and Ru/C-350), were subjected to temperature-programmed reduction (TPR). Samples were reduced by using a reductive mixture (10 mL/min of H_2 (5 vol%)-N_2) in a flow reactor by heating at 6 °C/min from 25 to 700 °C. The reactor outlet was connected to a thermal conductivity detector (TCD) in order to obtain the TPR signal.

Fourier transform infrared (FTIR) spectroscopy was used to elucidate the functional groups existing on the surface of ruthenium catalysts. Each sample (sample/KBr mass relationship 1:100) was grounded in a mortar, and 10 mm diameter wafers were pressed at 7.6 tonnes/cm^2. The spectra were obtained with Shimadzu FTIR Prestige-21 equipment, with a resolution of 4 cm^{-1} in the 500 to 4000 cm^{-1} range.

X-ray photoelectron spectroscopy (XPS) analysis was performed on SPECS equipment, with a dual Ag/Al monochromatic X-ray source and a PHOIBOS 150 hemispherical analyzer. Spectra were obtained with AlKα monochromatic radiation at 300 W. The step energy was 30 eV, and the fixed analyzer transmission mode (FAT) was used. Samples were supported on double-sided copper tape and subjected to ultra-high vacuum evacuation for at least 12 h prior to measurements.

2.3. Reactions

The hydrogenation reactions were carried out in a 100 mL Parr reactor, which was charged with 100 mg of catalyst, 33 mL of distilled water, and 2.3 g of levulinic acid. The system was heated to 70 °C, with a constant hydrogen pressure of 1.5 MPa and 1500 rpm stirring. The reaction time was 2 h.

The reactant (levulinic acid) and product (γ-valerolactone) concentration were determined by gas chromatography (Clarus 590, Perkin Elmer) using a 30 m × 0.32 mm × 0.25 μm

WaxPlus column and FID detector. Acetic acid was employed as an external standard (100 μL in 2 mL of reaction sample).

The levulinic acid conversion (X_{LA}), γ-valerolactone selectivity (S_{GVL}), and γ-valerolactone yield (η_{GVL}) were calculated using Equations (1)–(3), respectively:

$$X_{LA} = \frac{Moles\ of\ reacted\ LA}{Moles\ of\ initial\ LA} \times 100\% \tag{1}$$

$$S_{GVL} = \frac{Moles\ of\ produced\ GVL}{Moles\ of\ reacted\ LA} \times 100\% \tag{2}$$

$$\eta_{GVL} = \frac{Moles\ of\ produced\ GVL}{Moles\ of\ initial\ LA} \times 100\% \tag{3}$$

Separation of the solid catalyst was achieved through filtration. The recovered catalyst was washed with deionized water and ethanol and dried at 70 °C before being reused.

3. Results and Discussion

Table 1 shows the rice husk and hydrothermally activated carbon composition. Biomass residues are often analyzed for their elemental composition, which includes carbon, hydrogen, oxygen, and nitrogen, to evaluate their potential as a carbon precursor. Rice husk, for example, has a carbon content of nearly 40%, making it a viable option as a carbonaceous support [16]. The composition of the biomass reported in Table 1 is consistent with the TGA tests (see below), where the weight loss registered corresponds mainly to the thermal decomposition of hemicellulose (200–350 °C), cellulose (300–400 °C), and lignin (200–900 °C).

Table 1. Proximate and elemental analysis of VRH and HTC samples.

Biomass	VRH	HTC
Moisture content (wt.%)	8.6	5.2
Proximate analysis (wt.%, dry basis)		
Volatile matter	60.9	12.7
Ash content	23.1	51.0
Fixed carbon	15.9	36.3
Elemental analysis (wt.%, dry basis)		
Carbon	39.2	38.7
Hydrogen	4.4	1.7
Oxygen	32.9	8.1
Nitrogen	0.3	0.5

As can be observed in Figure 2a, the virgin rice husk presented a significant weight loss of 70% at 900 °C (in coincidence with the data reported in Table 1, i.e., 60.9% volatile and 8.6% moisture). Figure 2b illustrates that the weight reduction of the hydrothermally treated carbon was 18%. This aligned with the values presented in Table 1, indicating a volatility of 12.7% and moisture content of 5.2%. Previous studies showed that there are three main weight loss stages during the TGA analysis of activated carbon [50]. This fact is consistent with TGA results obtained in our study. The first weight loss stage occurs between 30 and 165 °C, with a 2% weight loss. This was attributed to the evaporation of water molecules adsorbed on the pore surface of the carbon [51]. The second weight loss stage occurs between 165 and 700 °C with a 3% weight loss, followed by another stage from 700 to 900 °C with a weight loss of 13%. The weight loss observed in these two stages can be attributed to the intensive gasification of the residual volatile organic compounds [52], as well as the breakdown of lignin-like structures [53].
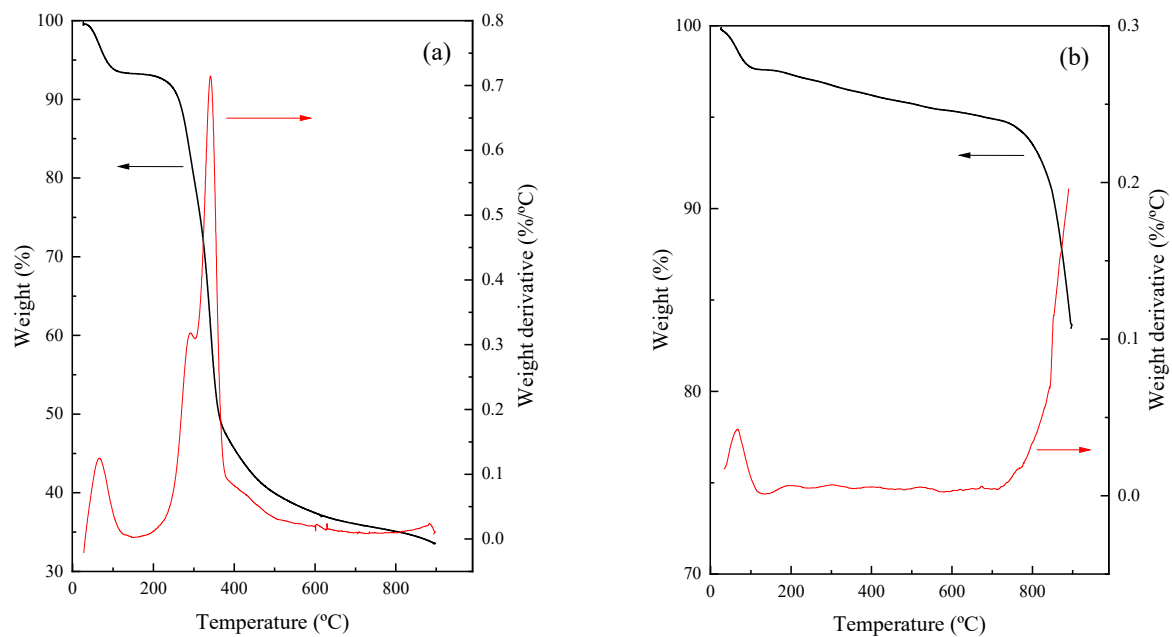
Figure 2. TGA/DTA profiles of (**a**) virgin rice husk (VRH) and (**b**) hydrothermally treated carbon (HTC).

The composition of the ashes was determined using X-ray fluorescence. It was found that it contained approximately 94.9% SiO_2, as well as minor amounts of K_2O, SO_3, CaO, MnO, Fe_2O_3, and ZnO.

Table 2 shows the values of BET-specific surface area (S_{BET}), total pore volume, and average mesopore diameter calculated by N_2 adsorption–desorption isotherms of virgin rice husk and hydrothermally treated carbon.

Table 2. Textural properties of virgin rice husk (VRH) and hydrothermally treated carbon (HTC).

Sample	S_{BET} (m^2/g)	Total Pore Volume (cm^3/g)	Average Pore Diameter (nm)
VRH	6	0.0097	10.2
HTC	158	0.0600	4.1

From the analysis of the adsorption–desorption isotherms of the materials (Figure 3), it can be seen that both VRH and HTC corresponded to a type II isotherm with a H4-type hysteresis loop, according to IUPAC, with parallel adsorption and desorption branches in the range of relative pressures from 0.4 to 1, thus showing that the material presented micro and mesoporosity. The specific surface area (S_{BET}) of the VRH sample was 6 m^2/g, and after activation with H_3PO_4, the HTC sample reached an area value of 158 m^2/g.

The notable increase in the specific surface area (25 times) was due to the activation process caused by the hydrothermal treatment using phosphoric acid and temperature. According to bibliography reports, phosphoric acid changes the structure of the pores in the samples with the consequent increase in the surface area [54,55]. Similar values of specific surfaces were reported by Mohammad et al. [56], who attributed the surface area increase to the impregnation with phosphoric acid and subsequent washing, which leads to the removal of unorganized carbon or residual tarry material at low temperatures, thus opening the closed pores [52,57], or to the elimination of soluble phosphates formed by the reaction of phosphoric acid and the silica present in the raw material [56].
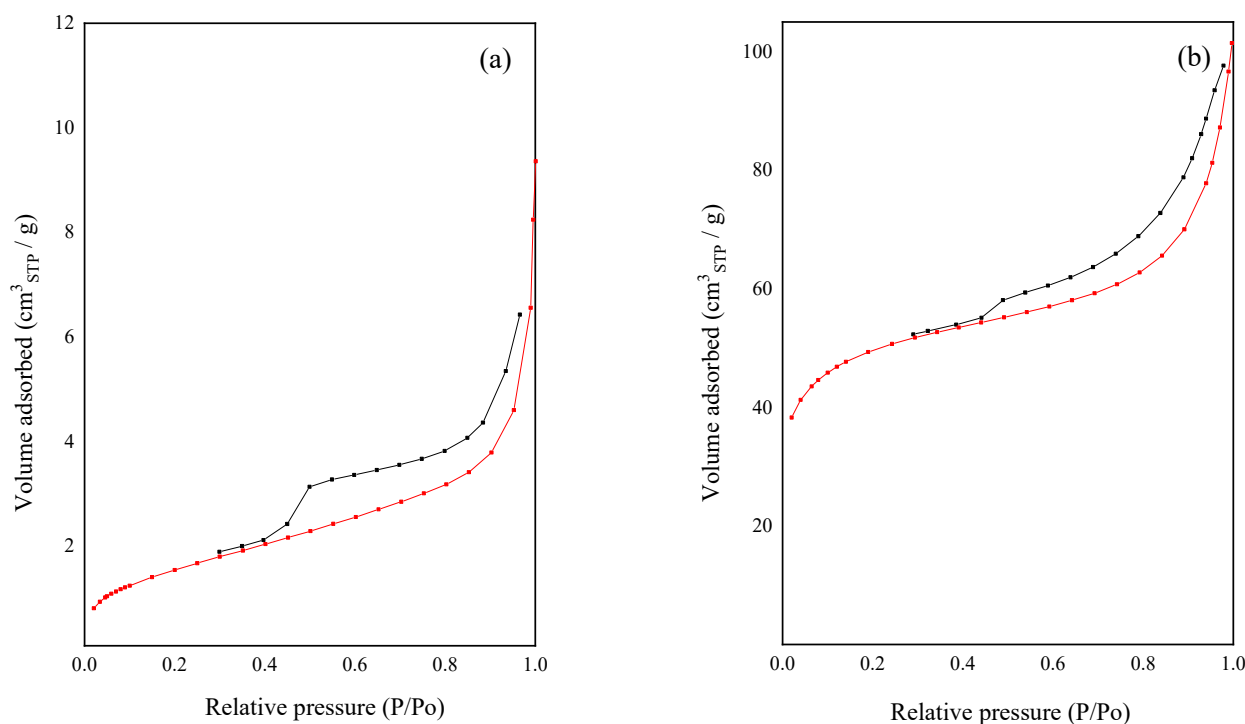
Figure 3. Nitrogen adsorption–desorption isotherms of (**a**) virgin rise husk (VRH) and (**b**) hydrothermally treated carbon (HTC).

Typically, during hydrothermal treatment, lignin is considered to be the least reactive fraction of biomass [58]. However, hydrothermal digestion of cellulose and hemicellulose produces intermediates (such as furfural) that can undergo further polymerization via dehydration reactions [58–60]. The presence of concentrated phosphoric acid creates a low-pH environment that promotes both the dehydration of cellulose and the saccharides into furfural [61], which is the initial stage in the hydrothermal carbonization of cellulose. Overall, the utilization of both H_3PO_4 and hydrothermal conditions is essential to enhance yield and encourage carbon fixation in biomass [16].

The catalysts' acidity was determined by the temperature-programmed desorption of pyridine, showing that the reduction process decreased the acidity with respect to the original sample (Ru/C). From Figure 4, it can be seen that the catalysts, after being impregnated with the metal precursor ($RuCl_3$) and reduced at 150 and 200 °C, had lower acidity (87.2–87.8 μmol Py/g cat, respectively) when compared to those treated at other temperatures such as 100, 275, and 350 °C, whose acidity values were 111.7, 97.6, and 103.7 μmolPy/g cat, respectively. This would indicate that the acidity depended closely on the temperature of the reduction treatment. In a recent investigation by Yu et al. [62], the impact of the acid characteristics of the support on the performance of bifunctional catalysts for the heterogeneous conversion of LA to GVL was studied. The researchers found that the acidity of the support is a crucial factor in this transformation, affecting both the metal dispersion and the catalyst's stability during mild reaction conditions.

The TPR profiles are shown in Figure 5 and are characteristic of supported ruthenium catalysts. Two very close peaks can be observed, one at 120 °C and the other at 178 °C. According to the literature, the first peak is attributed to the reduction of chlorinated species, while the second one corresponds to the reduction of ruthenium oxychloride [63,64]. Furthermore, the hydrogen consumption displayed between 300 and 400 °C corresponds to the methanation of carbon [65,66]. It was observed that as the reduction temperature increased, H_2 consumption decreased. The chlorinated species were easily reducible, and no signs of them were observed in the reduced catalysts at the temperatures used in this study.
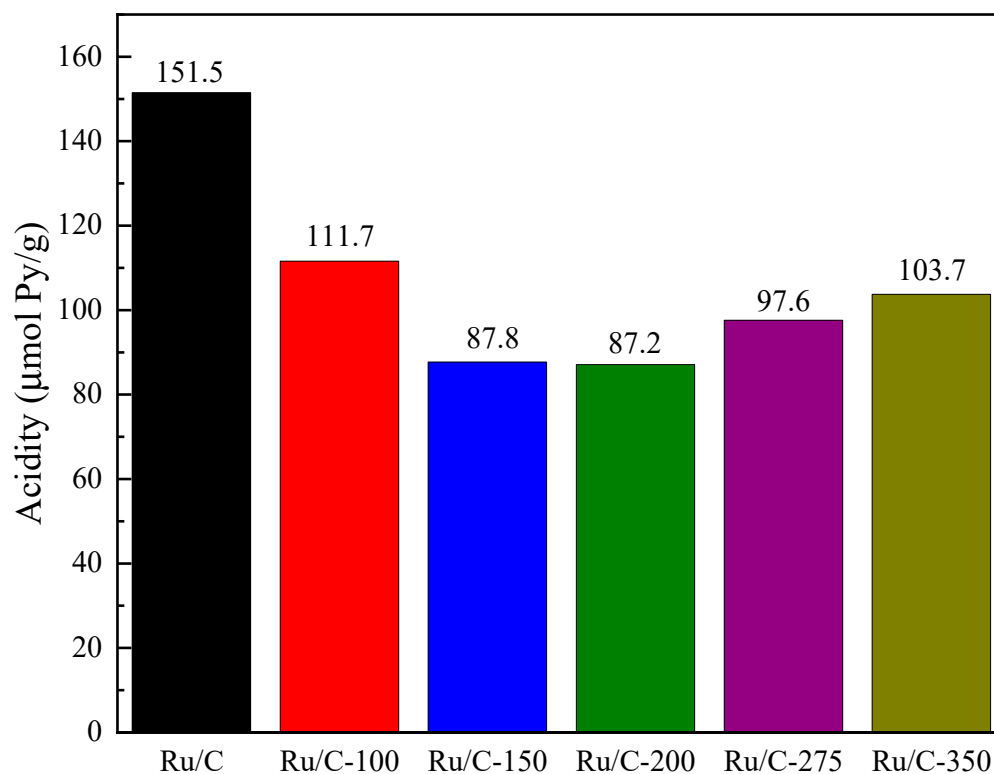
Figure 4. Total acidity measured by pyridine TPD of ruthenium supported on hydrothermally treated carbon (Ru/C) and the catalysts reduced at different temperatures (Ru/C-temp).

RuO_2 reduction by H_2 was initiated at temperatures between 50 to 200 °C due to the hydrogenation of surface oxygen atoms. The creation of oxygen vacancies, by desorbing water vapor, accelerated the reduction process by exchanging bulk oxygen atoms with the vacancies. In the range of 200 to 300 °C, the reduction was slow. Even though the creation of oxygen vacancies at bulk sites accelerates the reduction, the rate was slower than that in the 100 to 200 °C range. At temperatures between 300 and 400 °C, RuO_2 reduction began immediately upon exposure to H_2, and oxygen vacancies were created directly. The reduction rate increased with temperature, but not as fast as in the low-temperature range of 100 to 200 °C [67].

Figure 6 shows the FTIR spectra of the ruthenium catalysts supported on activated carbon after reduction at different temperatures. IR spectroscopy is a valuable tool for identifying the types of functional groups present on the catalyst surface. However, carbon-supported metal catalysts have been relatively underexplored due to the challenges of obtaining IR spectra from these opaque materials. Fortunately, the application of the carbon film technique has significantly improved the feasibility of experimental spectroscopic investigations of surface phenomena on carbons [68].

Surface functional groups can be observed (references to the different functional groups are identified by capital letters in Figure 6). The band at 3743 cm^{-1} (A), which is only present in the reduced catalysts, was due to ν(OH) vibrations of hydroxyl groups on the surface [69] and, probably, of water. The ν_3 absorption band of carbon dioxide (CO_2) can be observed at 2370–2378 cm^{-1} (B), and the band at 2312–2318 cm^{-1} (C) was assigned to the ν_3(OCO) [70]. Two bands with lower definition were observed at 1700 cm^{-1} (D) and 1650 cm^{-1} (E). The first one can be attributed to the stretch vibration of ν(RHC=O) [71], while the second was assigned to carbonate ν(CO) [72] and the stretch vibration of ν(C=C). A broad band in the range of 1510–1560 cm^{-1} was observed in the reduced catalysts, which can be assigned to the CO stretching vibrations of formate species on the reduced Ru [72]. This band was not significant in the unreduced sample (Ru/C). An intense band at 1182–1186 cm^{-1} (F) can be assigned to the stretch vibration of ν(–C–OH) [71]. It has been

mentioned that –C–OH groups are related to the reduction of ruthenium ions, and those groups can be adsorbed on the surface of Ru particles, avoiding their agglomeration [73]. Finally, the band at 1046 cm^{-1} (G) can be attributed to the stretching vibration of ν(–C–OH) [71,73–75]. Moreover, according to Wisniewski et al. [76], the signals in the 900–1300 cm^{-1} range can be attributed to ashes and phosphate species from the H_3PO_4 used during the hydrothermal process. Bourbigot et al. [77] identified species of the type ν_{as}(-P-O), ν_{sym}(-PO$_2$ and PO$_3$), and ν_{sym}(-P-O); stretching mode of P-O-C; and stretching mode in P=O in the same region.
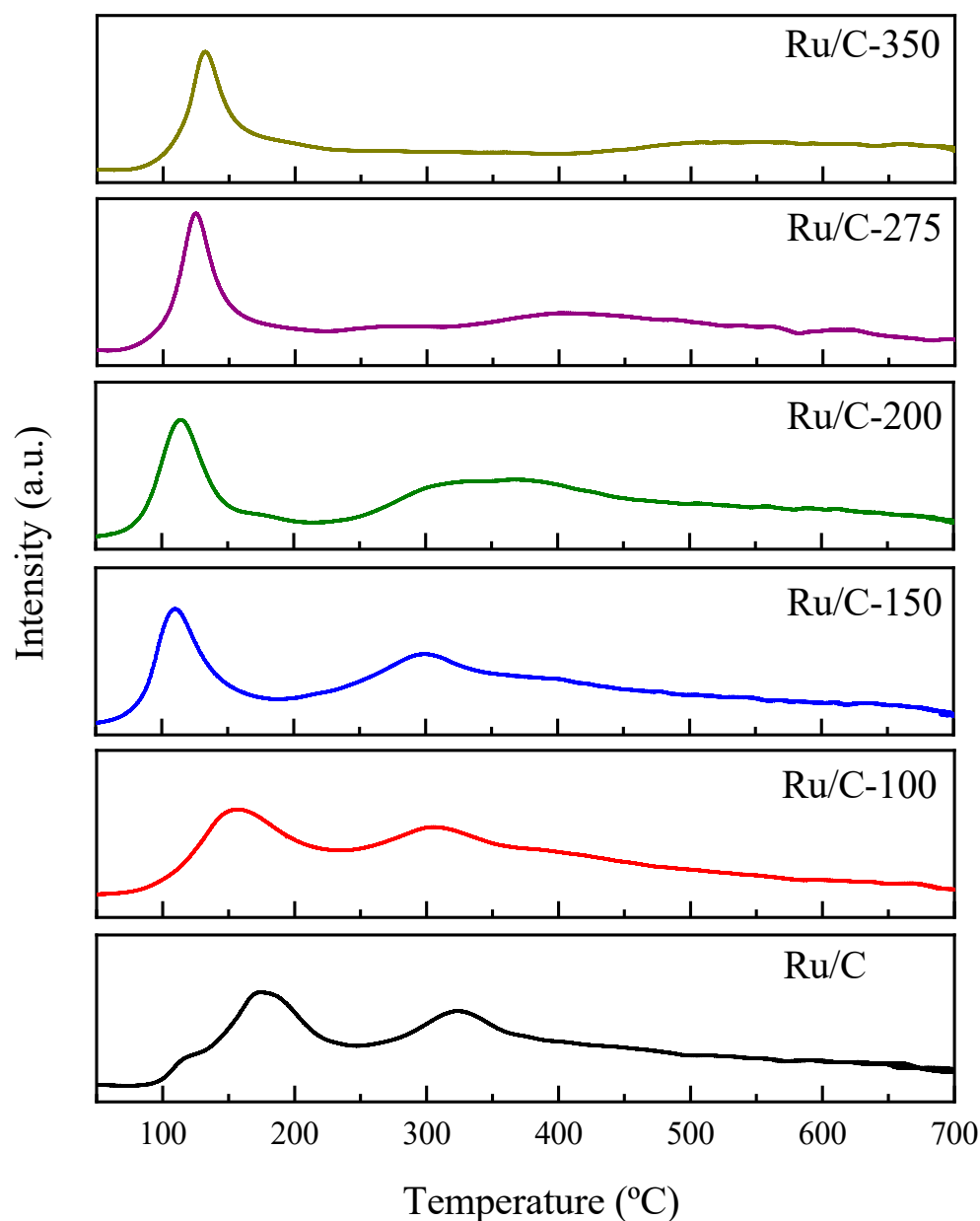

Figure 5. TPR profile of ruthenium supported on hydrothermally treated carbon (Ru/C) and the catalysts reduced at different temperatures (Ru/C-temp).

Some of the catalysts were evaluated by X-ray photoelectron spectroscopy. Since the Ru 3d signal interferes with the C 1s signal, it is very difficult to resolve the oxidation state of Ru in this region. Therefore, the Ru 3p signal was analyzed in order to differentiate the oxidation states of Ru in these samples. The obtained XPS spectra (Figure 7) showed that as the reduction temperature increased, there was a shift of the peaks towards the binding

energy that corresponded to metallic Ru. The catalyst that was reduced at 150 °C showed a Ru 3p3/2 binding energy of 463.4 eV, which corresponded to RuO_2, while the sample reduced at 200 °C presented two peaks: the major peak corresponded to RuO_2 specie, at a binding energy of 463.0 eV, and the lower intensity peak belonged to Ru^0 (at 461.3 eV) [78]. When the catalyst was reduced at 350 °C, the XPS signal was also able to be deconvoluted into two peaks, the major one corresponding to metallic Ru (461.4 eV) and the other to RuO_2 (463.1 eV).
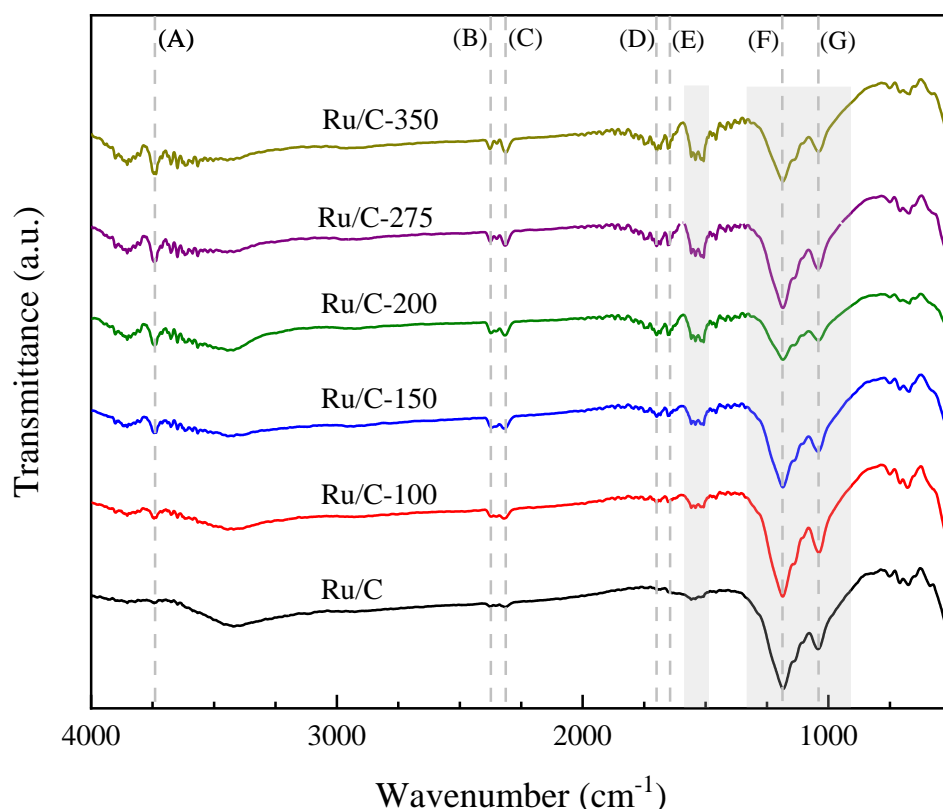

Figure 6. FTIR spectra of ruthenium supported on hydrothermally treated carbon (Ru/C) and the catalysts reduced at different temperatures (Ru/C-temp). Signals: (**A**) ν(OH) vibrations of hydroxyl groups; (**B**) ν_3 absorption band of CO_2; (**C**) ν_3(OCO); (**D**) stretch vibration of ν(RHC=O); (**E**) carbonate ν(CO) and stretch vibration of ν(C=C); (**F**) stretch vibration of ν(–C–OH); (**G**) stretching vibration of ν(–C–OH). Regions; 1560–1510 cm^{-1} range: CO stretching vibrations of formate species, 1300–900 cm^{-1} range: ashes and phosphate species.

Regarding the C 1s and O 1s signals (282.6 and 532.6 eV, respectively), the results suggest an O/C relationship of 0.85 for the sample Ru/C-150, a relationship of 0.65 for the case of Ru/C-200, and 0.41 for the case of Ru/C-350. These results are consistent with what the decomposition of the ruthenium peak yielded because as the temperature of reduction increased, the ratio of surface oxygen decreased due to the reducibility of the metal.

In order to determine the optimal reduction temperature of the metal (Ru) supported on hydrothermally activated carbon for the conversion of levulinic acid to γ-valerolactone, catalyst samples reduced at different temperatures were employed in the reaction, which was carried out at 1.5 MPa and 70 °C in an aqueous medium. In Figure 8, it can be seen that the reduction temperature of Ru presented an optimum, which maximized conversion and selectivity. Comparing the Ru-100, Ru-150, and Ru-200 samples, both conversion and selectivity increased with rising reduction temperatures. With the Ru-200 catalyst, the maximum conversion of levulinic acid (82%) and selectivity to the desired product (90%) were achieved. When the reduction temperature was increased to 275 and 350 °C, the conversion dropped sharply to values below 30%, and the selectivity fell slightly at

275 °C, while at 350 °C, it was almost negligible. This decrease in the catalyst performance could have been due to the formation of coke precursors [62] and the subsequent migration towards Ru active sites, as well as to a marked sintering of the metal, caused by the relatively high reduction temperature. It should be noted that the highest yield occurred for the Ru/C-200 catalyst that presented the lowest acidity value (Figure 4). A study conducted by Pan et al. [79] investigated the use of supported Ru catalysts for the hydrogenation of levulinic acid to valerate esters. The researchers found that as the amount of acid sites increased, the selectivity to GVL decreased.
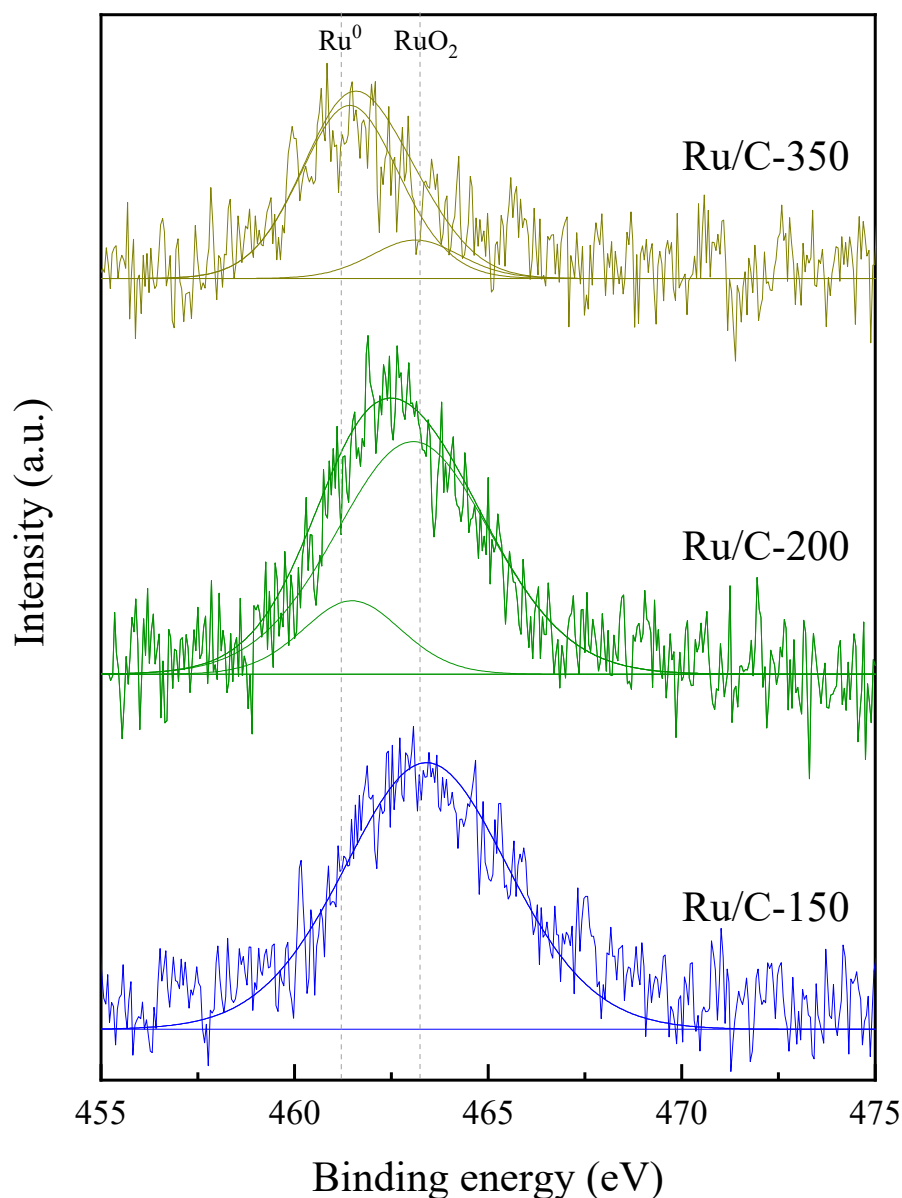

Figure 7. XPS spectra of the Ru 3p3/2 for Ru/C-150, Ru/C-200, and Ru/C-350 samples.

It should be noted that the acidity and oxidation state of the catalyst played a fundamental role in the levulinic acid hydrogenation reaction. Gundekari et al. [80] found that the zeolite-supported Ru catalyst was more active in the oxide form than in the metallic state for the hydrogenation reaction.

The role of the support in ruthenium heterogeneously catalyzed LA hydrogenation reaction is widely known. The LA carbonyl functionality is activated by the support, while the metal nanoparticles facilitate hydrogen activation.
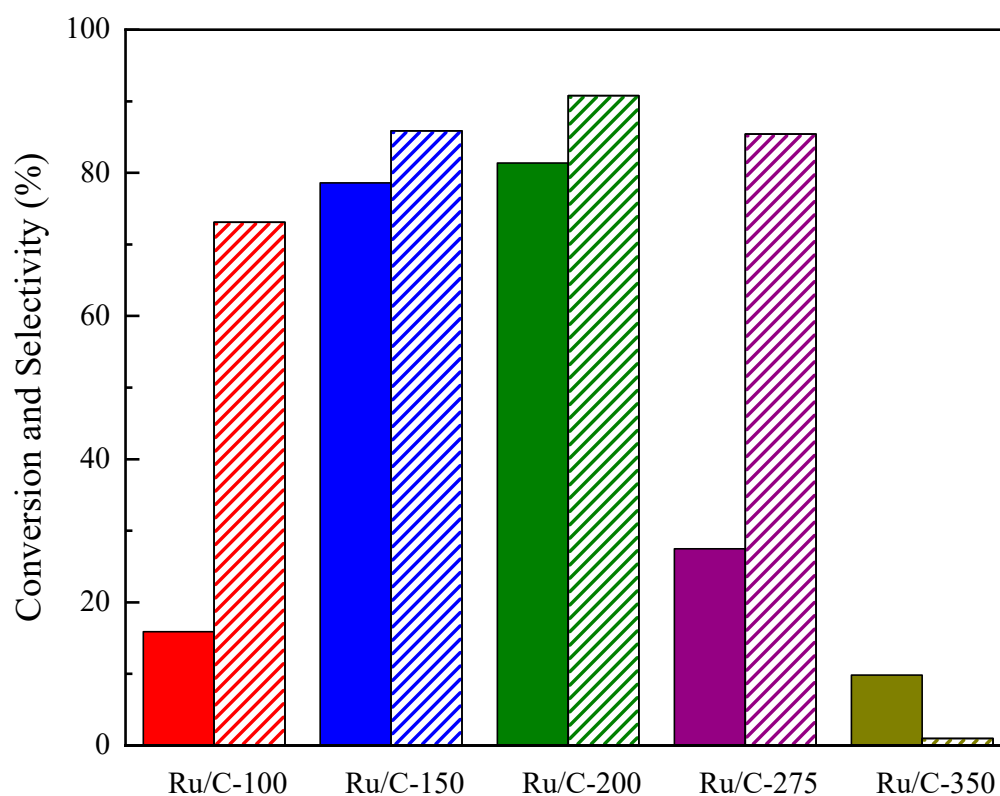
Figure 8. Levulinic acid conversion (full bars) and γ-valerolactone selectivity (dashed bars) of ruthenium supported on hydrothermally activated carbon catalysts reduced at different temperatures (Ru/C-temp).

The results of levulinic acid hydrogenation to γ-valerolactone using different supported Ru catalysts are presented in Table 3. As can be seen, the Ru/C-200 catalyst showed a similar performance to that of other ruthenium catalysts supported on different materials that have been reported in the literature for the moderate reaction conditions used in this work. It should be noted that the Ru/C-200 catalyst has a lower Ru content than the other catalysts supported on carbon, obtaining a higher yield.

Table 3. Ru-containing catalysts of LA hydrogenation supported on different materials.

Catalyst	Time (min)	Temperature (°C)	Pressure (MPa)	GVL Yield (%)	Ref.
5%Ru/SiO$_2$	160	130	1.2	75	[81]
5%Ru/Al$_2$O$_3$	160	130	1.2	76	[81]
5%Ru/ZSM-5C	240	70	3.0	93	[82]
1%Ru/H-β	120	90	4.5	66	[83]
3%Ru/HPNC	120	75	2.5	55	[84]
5%Ru/C	720	180	3.0	57	[85]
2%Ru/C-200	120	70	1.5	74	This work

The stability of the Ru/C-200 catalyst was investigated by reusing it for three reaction cycles. After each run, the catalyst was washed with water and ethanol, dried at 80 °C, and loaded to the next reaction cycle.

It was found that the catalyst retained good catalytic activity and selectivity (see Table 4) after three reaction cycles. LA conversion and selectivity to GVL decreased by approximately 12% after the third cycle. The decrease in activity could have been due to blockages of some active metal centers caused by the adsorption of reagents or reaction

products. Studies on catalyst recycling have demonstrated the robustness of these catalysts, indicating their potential for use in industrial applications.

Table 4. Levulinic acid conversion (X_{LA}), γ-valerolactone selectivity (S_{GVL}), and γ-valerolactone yield (η_{GVL}) of the Ru/C-200 catalyst in the different reuse cycles.

Run	X_{LA} (%)	S_{GVL} (%)	η_{GVL} (%)
1	82	90	74
2	78	82	64
3	72	78	56

4. Conclusions

Activated carbon was prepared from rice husk by hydrothermal treatment. The mentioned material was used as a support for ruthenium catalysts that were utilized in the hydrogenation reaction of levulinic acid to γ-valerolactone. The metal/acid bifunctionality required for this type of reaction could be achieved satisfactorily. In addition, an optimal reduction temperature of the Ru metal precursor was found, in order to maximize LA conversion and selectivity to the desired product (GVL). For the catalyst whose reduction temperature was 200 °C (Ru/C-200), a conversion of 82% with a GVL yield equal to 74% was obtained.

The operating conditions for the reaction carried out were mild (70 °C and 1.5 MPa) and fell within the range of those reported in the bibliography. It should be noted that the highest yield occurred for the Ru/C-200 catalyst that presented the lowest acidity and a high proportion of RuO_2. The catalyst showed satisfactory performance when it was reused in three reaction cycles.

Author Contributions: Conceptualization, V.I.R. and N.S.V.; methodology, V.I.R., G.M., B.S.S., J.R.G., R.A.P. and N.S.V.; validation, V.I.R. and N.S.V.; formal analysis, V.I.R., J.R.G. and N.S.V.; investigation, V.I.R., G.M., B.S.S., J.R.G., R.A.P. and N.S.V.; data curation, V.I.R., J.R.G. and N.S.V.; writing—original draft preparation, V.I.R., J.R.G. and N.S.V.; writing—review and editing, V.I.R., B.S.S., J.R.G. and N.S.V.; visualization, V.I.R.; supervision, S.R.d.M. and N.S.V.; project administration, N.S.V.; funding acquisition, J.R.G., S.R.d.M. and N.S.V. All authors have read and agreed to the published version of the manuscript.

Institutional Review Board Statement: Not applicable.

Informed Consent Statement: Not Applicable.

Data Availability Statement: Not applicable.

Conflicts of Interest: The authors declare no conflict of interest.

References

1. Vispute, T.P.; Zhang, H.Y.; Sanna, A.; Xiao, R.; Huber, G.W. Renewable chemical commodity feedstocks from integrated catalytic processing of pyrolysis oils. *Science* **2010**, *330*, 1222–1227. [CrossRef] [PubMed]
2. Stocker, M. Biofuels and biomass-to-liquid fuels in the biorefinery: Catalytic conversion of lignocellulosic biomass using porous materials. *Angew Chem. Int. Ed.* **2008**, *47*, 9200–9211. [CrossRef] [PubMed]
3. Wong, S.; Ngadi, N.; Inuwa, I.M.; Hassan, O. Recent advances in applications of activated carbon from biowaste for wastewater treatment: A short review. *J. Clean. Prod.* **2018**, *175*, 361–375. [CrossRef]
4. Villota, E.M.; Lei, H.; Qian, M.; Yang, Z.; Villota, S.M.A.; Zhang, Y.; Yadavalli, G. Optimizing microwave-assisted pyrolysis of phosphoric acid-activated biomass: Impact of concentration on heating rate and carbonization time. *ACS Sustain. Chem. Eng.* **2017**, *6*, 1318–1326. [CrossRef]
5. Chingombe, P.; Saha, B.; Wakeman, R.J. Surface modification and characterisation of a coal-based activated carbon. *Carbon* **2005**, *43*, 3132–3143. [CrossRef]

6. Yu, X.; Wang, S.; Zhang, J. Preparation of high adsorption performance activated carbon by pyrolysis of waste polyester fabric. *J. Mater. Sci.* **2018**, *53*, 5458–5466. [CrossRef]

7. Zhang, P.; Zhu, H.; Dai, S. Porous Carbon Supports: Recent Advances with Various Morphologies and Compositions. *ChemCatChem* **2015**, *7*, 2788–2805. [CrossRef]

8. Iwanow, M.; Gärtner, T.; Sieber, V.; König, B. Activated carbon as catalyst support: Precursors, preparation, modification and characterization. *Beilstein J. Org. Chem.* **2020**, *16*, 1188–1202. [CrossRef]

9. Shetty, A.; Molahalli, V.; Sharma, A.; Hegde, G. Biomass-Derived Carbon Materials in Heterogeneous Catalysis: A Step towards Sustainable Future. *Catalysts* **2023**, *13*, 20. [CrossRef]

10. Zubrik, A.; Matik, M.; Hredzak, S.; Lovás, M.; Danková, Z.; Kovácová, M.; Briancin, J. Preparation of chemically activated carbon from waste biomass by singlestage and two-stage pyrolysis. *J. Clean. Prod.* **2017**, *143*, 643–653. [CrossRef]

11. García, J.R.; Sedran, U.; Ahmad Zaini, M.A.; Akmar Zakaria, Z. Preparation, characterization, and dye removal study of activated carbon prepared from palm kernel shell. *Environ. Sci. Pollut. Res.* **2018**, *25*, 5076–5085. [CrossRef] [PubMed]

12. Namane, A.; Mekarzia, A.; Benrachedi, K.; Belhaneche-Bensemra, N.; Hellal, A. Determination of the adsorption capacity of activated carbon made from coffee grounds by chemical activation with $ZnCl_2$ and H_3PO_4. *J. Hazard. Mater.* **2005**, *119*, 189–194. [CrossRef] [PubMed]

13. Fu, Y.; Shen, Y.; Zhang, Z.; Ge, X.; Chen, M. Activated biochars derived from rice husk via one- and two-step KOH catalyzed pyrolysis for phenol adsorption. *Sci. Total Environ.* **2019**, *646*, 1567–1577. [CrossRef] [PubMed]

14. Li, Y.; Zhang, X.; Yang, R.; Li, G.; Hu, C. The role of H_3PO_4 in the preparation of activated carbon from NaOH treated rice husk residue. *RSC Adv.* **2015**, *5*, 32626–32636. [CrossRef]

15. Titirici, M.M.; Antonietti, M. Chemistry and materials options of sustainable carbon materials made by hydrothermal carbonization. *Chem. Soc. Rev.* **2010**, *39*, 103–116. [CrossRef] [PubMed]

16. Quesada-Plata, F.; Ruiz-Rosas, R.; Morallón, E.; Cazorla-Amorós, D. Activated carbons prepared through H_3PO_4-assisted hydrothermal carbonization from biomass wastes: Porous texture and electrochemical performance. *ChemPlusChem* **2016**, *81*, 1349–1359. [CrossRef]

17. Xue, Z.; Jiang, J.; Li, G.; Zhao, W.; Wang, J.; Mu, T. Zirconium-cyanuric acid coordination polymer: Highly efficient catalyst for conversion of levulinic acid to γ-valerolactone. *Catal. Sci. Technol.* **2016**, *6*, 5374–5379. [CrossRef]

18. Luan, Q.J.; Liu, L.J.; Gong, S.W.; Lu, J.; Wang, X.; Lv, D.M. Clean and efficient conversion of renewable levulinic acid to levulinate esters catalyzed by an organic-salt of $H_4SiW_{12}O_{40}$. *Process Saf. Environ. Prot.* **2018**, *117*, 341–349. [CrossRef]

19. Albani, D.; Li, Q.; Vilé, G.; Mitchell, S.; Almora-Barrios, N.; Witte, P.T.; López, N.; Pérez-Ramírez, J. Interfacial acidity in ligand-modified ruthenium nanoparticles boosts the hydrogenation of levulinic acid to gamma-valerolactone. *Green Chem.* **2017**, *19*, 2361–2370. [CrossRef]

20. Fang, S.; Cui, Z.; Zhu, Y.; Wang, C.; Bai, J.; Zhang, X.; Xu, Y.; Liu, Q.; Chen, L.; Zhang, Q.; et al. In situ synthesis of biomass-derived Ni/C catalyst by self-reduction for the hydrogenation of levulinic acid to γ–valerolactone. *J. Energy Inst.* **2019**, *37*, 204–214. [CrossRef]

21. Wang, S.; Dorcet, V.; Roisnel, T.; Bruneau, C.; Fischmeister, C. Ruthenium and Iridium Dipyridylamine Catalysts for the Efficient Synthesis of γ-Valerolactone by Transfer Hydrogenation of Levulinic Acid. *Organometallics* **2017**, *36*, 708–713. [CrossRef]

22. Orlowski, I.; Douthwaite, M.; Iqbal, S.; Hayward, J.S.; Davies, T.E.; Bartley, J.K.; Miedziak, P.J.; Hirayama, J.; Morgan, D.J.; Willock, D.J.; et al. The hydrogenation of levulinic acid to γ-valerolactone over Cu–ZrO_2 catalysts prepared by a pH-gradient methodology. *J. Energy Chem.* **2019**, *36*, 15–24. [CrossRef]

23. Schutte, H.A.; Thomas, R.W. Normal valerolactone. iii. Its preparation by the catalytic reduction of levulinic acid with hydrogen in the presence of platinum oxide. *J. Am. Chem. Soc.* **1930**, *52*, 3010–3012. [CrossRef]

24. Christian, R.V.; Brown, H.D.; Hixon, R.M. Derivatives of γ-valerolactone, 1,4-pentanediol and 1,4-Di-(β-cyanoethoxy)-pentane. *J. Am. Chem. Soc.* **1947**, *69*, 1961–1963. [CrossRef]

25. Wang, J.; Wang, Y.; Tong, X.; Wang, Y.; Jin, G.; Guo, X. Highly active Ir/SiC catalyst for aqueous hydrogenation of levulinic acid to γ-valerolactone. *Catal. Commun.* **2020**, *139*, 105971–105975. [CrossRef]

26. Du, X.; Liu, Y.; Wang, J.; Cao, Y.; Fan, K. Catalytic conversion of biomass-derived levulinic acid into γ-valerolactone using iridium nanoparticles supported on carbon nanotubes. *Chin. J. Catal.* **2013**, *34*, 993–1001. [CrossRef]

27. Shen, L.; Zheng, Q.; Liu, Y.; Wu, J.; Lua, Z.; Tu, T. Efficient hydrogenation of levulinic acid catalysed by spherical NHC-Ir assemblies with atmospheric pressure of hydrogen. *Green Chem.* **2021**, *23*, 5037–5042. [CrossRef]

28. Amarasekara, A.S.; Hasan, M.A. Pd/C catalyzed conversion of levulinic acid to γ-valerolactone using alcohol as a hydrogen donor under microwave conditions. *Catal. Commun.* **2015**, *60*, 5–7. [CrossRef]

29. Damayanti, A.P.; Dewi, H.P. Selective hydrogenation of levulinic acid to γ-valerolactone using bimetallic Pd-Fe catalyst supported on titanium oxide. *IOP Conf. Ser.: Mater. Sci. Eng.* **2020**, *980*, 012013. [CrossRef]

30. Feng, J.; Li, M.; Zhong, Y.; Xu, Y.; Meng, X.; Zhao, Z.; Feng, C. Hydrogenation of levulinic acid to γ-valerolactone over Pd@UiO-66-NH2 with high metal dispersion and excellent reusability. *Microporous Mesoporous Mater.* **2020**, *294*, 109858–109867. [CrossRef]

31. Parapat, R.Y.; Yudatama, F.A.; Musadi, M.R.; Schwarze, M.; Schomacker, R. Antioxidant as structure directing agent in nanocatalyst preparation. Case study: Catalytic activity of supported Pt nanocatalyst in levulinic acid hydrogenation. *Ind. Eng. Chem. Res.* **2019**, *58*, 2460–2470. [CrossRef]

32. Wang, Y.; Bao, J.; Zuo, C.; Dong, G.; Sheng, X.; Huang, Y.; Zhang, Y.; Zhou, Y. Ultra-small PtNi bimetallic encapsulated in silicalite-1zeolite with fine-tuned surface acidity for selective conversion of levulinic acid. *Appl Organomet Chem.* **2023**, *37*, e6935. [CrossRef]

33. Meng, F.; Yang, X.; Zhao, S.; Li, Z.; Zhang, G.; Qi, Y.; Chu, S.; Wang, G.; Zhang, J.; Qin, Y.; et al. Shifting reaction path for levulinic acid aqueous-phase hydrogenation by Pt-TiO$_2$ metal-support interaction. *Appl. Catal. B Environ.* **2023**, *324*, 122236–122245. [CrossRef]

34. Upare, P.P.; Lee, J.-M.; Hwang, D.W.; Halligudi, S.B.; Hwang, Y.K.; Chang, J.-S. Selective hydrogenation of levulinic acid to γ-valerolactone over carbon-supported noble metal catalysts. *J. Ind. Eng. Chem.* **2011**, *17*, 287–292. [CrossRef]

35. Seretis, A.; Diamantopoulou, P.; Thanou, I.; Tzevelekidis, P.; Fakas, C.; Lilas, P.; Papadogianakis, G. Recent advances in ruthenium-catalyzed hydrogenation reactions of renewable biomass-derived levulinic acid in aqueous media. *Front. Chem.* **2020**, *8*, 221–243. [CrossRef] [PubMed]

36. Manzer, L.E. Catalytic synthesis of α-methylene-γ-valerolactone: A biomass-derived acrylic monomer. *Appl. Catal. A Gen.* **2004**, *272*, 249–256. [CrossRef]

37. Manzer, L.E. Production of 5-Methylbutyrolactone from Levulinic Acid. US Patent 6617464 B2, 9 September 2003. Available online: https://patentimages.storage.googleapis.com/a8/d5/42/16a704c75f7ce5/US6617464.pdf (accessed on 1 March 2023).

38. Manzer, L.E.; Hutchenson, K.W. Production of 5-methyl-dihydro-furan-2-one from Levulinic Acid Supercritical Media. US Patent 6946563 B2, 20 September 2005.

39. Bourne, R.A.; Stevens, J.G.; Ke, J.; Poliakoff, M. Maximising opportunities in supercritical chemistry: The continuous conversion of levulinic acid to γ-valerolactone in CO$_2$. *Chem. Commun.* **2007**, *44*, 4632–4634. [CrossRef] [PubMed]

40. Yan, Z.P.; Lin, L.; Liu, S. Synthesis of γ-Valerolactone by Hydrogenation of Biomass-derived Levulinic Acid over Ru/C Catalyst. *Energy Fuels* **2009**, *23*, 3853–3858. [CrossRef]

41. Tan, J.; Cui, J.; Cui, X.; Deng, T.; Li, X.; Zhu, Y.; Li, Y. Graphene-Modified Ru Nanocatalyst for Low-Temperature Hydrogenation of Carbonyl Groups. *ACS Catal.* **2015**, *5*, 7379–7384. [CrossRef]

42. Ftouni, J.; Muñoz-Murillo, A.; Goryachev, A.; Hofmann, J.P.; Hensen, E.J.M.; Lu, L.; Kiely, C.J.; Bruijnincx, P.C.A.; Weckhuysen, B.M. ZrO$_2$ Is Preferred over TiO$_2$ as Support for the Ru-Catalyzed Hydrogenation of Levulinic Acid to γ-Valerolactone. *ACS Catal.* **2016**, *6*, 5462–5472. [CrossRef]

43. Cao, S.; Monnier, J.R.; Regalbuto, J.R. Alkali promotion of alumina-supported ruthenium catalysts for hydrogenation of levulinic acid to γ-valerolactone. *J. Catal.* **2017**, *347*, 72–78. [CrossRef]

44. Cao, W.; Luo, W.; Ge, H.; Su, Y.; Wang, A.; Zhang, T. UiO-66 derived Ru/ZrO$_2$@C as a highly stable catalyst for hydrogenation of levulinic acid to γ-valerolactone. *Green Chem.* **2017**, *19*, 2201–2211. [CrossRef]

45. Wang, R.; Chen, L.; Zhang, X.; Zhang, Q.; Li, Y.; Wang, C.; Ma, L. Conversion of levulinic acid to g-valerolactone over Ru/Al$_2$O$_3$–TiO$_2$ catalyst under mild conditions. *RSC Adv.* **2018**, *8*, 40989–40995. [CrossRef] [PubMed]

46. Li, S.; Wang, Y.; Yang, Y.; Chen, B.; Tai, J.; Liu, H.; Han, B. Conversion of levulinic acid to γ valerolactone over ultra-thin TiO$_2$ nanosheets decorated with ultrasmall Ru nanoparticle catalysts under mild condition. *Green Chem.* **2019**, *21*, 770–774. [CrossRef]

47. Liu, X.; Lan, G.; Su, P.; Qia, L.; Ramirez Reina, T.; Wang, L.; Li, X.; Liu, J. Highly stable Ru nanoparticles incorporated in mesoporous carbon catalysts for production of γ-valerolactone. *Catal. Today* **2020**, *351*, 75–82. [CrossRef]

48. Wang, F.; Shi, R.; Zhou, G. Manipulating the interfacial species on carbon nanospheres supported nanoparticulate Ru to boost the electronic metal support interaction for enhancing selective hydrogenation of levulinic acid. *Appl. Surf. Sci.* **2022**, *588*, 152913–152926. [CrossRef]

49. Channiwala, S.A.; Parikh, P.P. A unified correlation for estimating HHV of solid, liquid and gaseous fuels. *Fuel* **2002**, *81*, 1051–1063. [CrossRef]

50. Muniandy, L.; Adam, F.; Mohamed, A.R.; Ng, E.P. The synthesis and characterization of high purity mixed microporous/mesoporous activated carbon from rice husk using chemical activation with NaOH and KOH. *Microporous Mesoporous Mater.* **2014**, *197*, 316–323. [CrossRef]

51. Abdel-Nasser, A. An insight into the KOH activation mechanism through the production of microporous activated carbon for the removal of Pb2+ cations. *Appl. Surf. Sci.* **2009**, *255*, 3723–3730.

52. Somasundaram, S.; Sekar, K.; Gupta, V.K.; Ganesan, S. Synthesis and characterization of mesoporous activated carbon from rice husk for adsorption of glycine from alcohol-aqueous mixture. *J. Mol. Liq.* **2013**, *177*, 416–425. [CrossRef]

53. Kastanaki, E.; Vamvuka, D.; Grammelis, P.; Kakaras, E. Thermogravimetric studies of the behavior of lignite–biomass blends during devolatilization. *Fuel Process. Technol.* **2002**, *77*, 159–166. [CrossRef]

54. Luo, Y.; Li, D.; Chen, Y.; Sun, X.; Cao, Q.; Liu, X. The performance of phosphoric acid in the preparation of actived carbon-containing phosphorus species from rice husk. *J. Mater. Sci.* **2019**, *54*, 5008–5021. [CrossRef]

55. Cordero-Lanzac, T.; Rodriguéz-Mirasol, J.; Cordero, T.; Bilbao, J. Advances and Challenges in the Valorization of Bio-Oil: Hydrodeoxygenation Using Carbon-Supported Catalysts. *Energy Fuels* **2021**, *35*, 17008–17031. [CrossRef]

56. Mohammad, Y.S.; Shaibu-Imodagbe, E.M.; Igboro, S.B.; Giwa, A.; Okuofu, C.A. Effect of Phosphoric Acid Modification on Characteristics of Rice Husk Activated Carbon. *Irani. J. Energy Environ.* **2015**, *6*, 20–25.

57. Rosas, J.; Bedia, J.; Rodríguez-Mirasol, J.; Cordero, T. HEMP-derived activated carbon fibers by chemical activation with phosphoric acid. *Fuel* **2009**, *88*, 19–26. [CrossRef]

58. Kang, S.; Li, X.; Fan, J.; Chang, J. Characterization of Hydrochars Produced by Hydrothermal Carbonization of Lignin, Cellulose, d-Xylose, and Wood Meal. *Ind. Eng. Chem. Res.* **2012**, *51*, 9023–9031. [CrossRef]

59. Sevilla, M.; Fuertes, A.B. The production of carbon materials by hydrothermal carbonization of cellulose. *Carbon* **2009**, *47*, 2281–2289. [CrossRef]

60. Falco, C.; Baccile, N.; Titirici, M.M. Morphological and structural differences between glucose, cellulose and lignocellulosic biomass derived hydrothermal carbons. *Green Chem.* **2011**, *13*, 3273–3281. [CrossRef]

61. Titirici, M.M.; White, R.J.; Falco, C.; Sevilla, M. Black perspectives for a green future: Hydrothermal carbons for environment protection and energy storage. *Energy Environ. Sci.* **2012**, *5*, 6796–6822. [CrossRef]

62. Yu, Z.; Lu, X.; Bai, H.; Xiong, J.; Feng, W.; Ji, N. Effects of solid acid supports on the bifunctional catalysis of levulinic acid to γ-valerolactone: Catalytic activity and stability. *Chem. Asian J.* **2020**, *15*, 1182–1201. [CrossRef] [PubMed]

63. Almeida, L.A.; Rocha, A.L.A.; Rodrigues, T.S.; Robles-Azocar, P.A. Highly selective hydrogenation of levulinic acid catalyzed by Ru on TiO2-SiO2 hybrid support. *Catal. Today* **2020**, *344*, 158–165. [CrossRef]

64. Mazzieri, V.A.; Sad, M.R.; Vera, C.R.; Pieck, C.L. Preparation and characterization of Ru-Sn/Al$_2$O$_3$ catalysts for the hydrogenation of fatty acid methyl esters. *Quim. Nova* **2010**, *33*, 269–272. [CrossRef]

65. García-García, F.R.; Gallegos-Suarez, E.; Fernández-García, M.; Guerrero-Ruiz, A.; Rodríguez-Ramos, I. Understanding the role of oxygen surface groups: The key for a smart ruthenium-based carbon-supported heterogeneous catalyst design and synthesis. *Appl. Catal. A-Gen.* **2017**, *544*, 66–76. [CrossRef]

66. Lan, G.; Tang, H.; Zhou, Y.; Han, W.; Liu, H.; Li, H.; Li, Y. Direct Synthesis of Ruthenium-Containing Ordered Mesoporous Carbon with Tunable Embedding Degrees by Using a Boric Acid-Assisted Approach. *ChemCatChem* **2014**, *6*, 353–360. [CrossRef]

67. Ugur, D.; Storm, A.J.; Verberk, R.; Brouwer, J.C.; Sloof, W.G. Kinetics of Reduction of a RuO$_2$(110) Film on Ru(0001) by H$_2$. *J. Phys. Chem. C* **2012**, *116*, 26822–26828. [CrossRef]

68. Wisniewski, M.; Zawadzki, J. Reduction of NO by H$_2$ on carbon film supported Ni catalysts—In situ FTIR study. *Catal. Lett.* **2004**, *94*, 135–141. [CrossRef]

69. Choe, S.J.; Kang, H.J.; Kim, S.J.; Park, S.B.; Park, D.H.; Huh, S.D. Adsorbed Carbon Formation and Carbon Hydrogenation for CO$_2$ Methanation on the Ni(111) Surface: ASED-MO Study. *Bull. Korean Chem. Soc.* **2005**, *26*, 1682–1688.

70. Bennett, C.J.; Hama, T.; Kim, Y.S.; Kawasaki, M.; Kaiser, R.I. Laboratory studies on the formation of formic acid (HCOOH) in interstellar and cometary ices. *Astrophys. J.* **2011**, *27*, 727–741. [CrossRef]

71. Chen, H.; Wang, J.; Huang, D.; Chen, X.; Zhu, J.; Sun, D.; Huang, J.; Li, Q. Plant-mediated synthesis of size-controllable Ni nanoparticles with alfalfa extract. *Mater. Lett.* **2014**, *122*, 166–169. [CrossRef]

72. Zheng, J.; Wang, C.; Chu, W.; Zhou, Y.; Kohler, K. CO$_2$ Methanation over Supported Ru/Al$_2$O$_3$ Catalysts: Mechanistic Studies by In situ Infrared Spectroscopy. *Chem. Select.* **2016**, *1*, 3197–3203.

73. Ma, Y.; Huang, Y.; Cheng, Y.; Wang, L.; Li, X. Biosynthesized ruthenium nanoparticles supported on carbon nanotubes as efficient catalysts for hydrogenation of benzene to cyclohexane: An eco-friendly and economical bioreduction method. *Appl. Catal. A-Gen.* **2014**, *484*, 154–160. [CrossRef]

74. Yang, X.; Li, Q.; Wang, H.; Huang, J.; Lin, L.; Wang, W.; Sun, D.; Su, Y.; Berya Opiyo, J.; Hong, L.; et al. Green synthesis of palladium nanoparticles using broth of Cinnamomum camphora leaf. *J. Nanopart. Res.* **2010**, *12*, 1589–1598. [CrossRef]

75. Stuart, B. *Infrared Spectroscopy: Fundamentals and Applications*; Wiley-VCH Verlag Gmbh & Co. KGaA: Weinheim, Germany, 2004; pp. 1–208.

76. Wisniewski, M.; Pacholczyk, A.; Terzyk, A.P.; Rychlicki, G. New phosphorus-containing spherical carbon adsorbents as promising materials in drug adsorption and release. *J. Colloid Interface Sci.* **2011**, *354*, 891–894. [CrossRef] [PubMed]

77. Bourbigot, S.; Le Bras, M.; Delobel, R. Carbonization mechanisms resulting from intumescence—Part ii. Association with an ethylene terpolymer and the ammonium polyphosphate-pentaerythritol fire retardant system. *Carbon* **1995**, *33*, 283–294. [CrossRef]

78. Iqbal, S.; Kondrat, S.A.; Jones, D.R.; Schoenmakers, D.C.; Edwards, J.K.; Lu, L.; Yeo, B.R.; Wells, P.P.; Gibson, E.K.; Morgan, D.J.; et al. Ruthenium Nanoparticles Supported on Carbon: An Active Catalyst for the Hydrogenation of Lactic Acid to 1,2-Propanediol. *ACS Catal.* **2015**, *5*, 5047–5059. [CrossRef]

79. Pan, T.; Deng, J.; Xu, Q.; Xu, Y.; Guo, Q.-X.; Fu, Y. Catalytic conversion of biomass-derived levulinic acid to valerate esters as oxygenated fuels using supported ruthenium catalysts. *Green Chem.* **2013**, *15*, 2967–2974. [CrossRef]

80. Gundekari, S.; Srinivasana, K. Hydrous ruthenium oxide: A new generation remarkable catalyst precursor for energy efficient and sustainable production of γ-valerolactone from levulinic acid in aqueous medium. *Appl. Catal. A-Gen.* **2019**, *569*, 117–125. [CrossRef]

81. Al-Shaal, M.G.; Wright, W.R.H.; Palkovits, R. Exploring the ruthenium catalysed synthesis of γ-valerolactone in alcohols and utilisation of mild solvent-free reaction conditions. *Green Chem.* **2012**, *14*, 1260–1263. [CrossRef]

82. Zhang, B.; Wu, Q.; Zhang, C.; Su, X.; Shi, R.; Lin, W.; Li, Y.; Zhao, F. A Robust Ru/ZSM-5 Hydrogenation Catalyst: Insights into the Resistances to Ruthenium Aggregation and Carbon Deposition. *ChemCatChem* **2017**, *9*, 3646–3654. [CrossRef]

83. Piskun, A.; Winkelman, J.G.M.; Tang, Z.; Heeres, H.J. Support Screening Studies on the Hydrogenation of Levulinic Acid to γ-Valerolactone in Water Using Ru Catalysts. *Catalysts* **2016**, *6*, 131. [CrossRef]

84. Li, B.; Zhao, H.; Fang, J.; Li, J.; Gao, W.; Ma, K.; Liu, C.; Yang, H.; Ren, X.; Dong, Z. Ru nanoparticles anchored on porous N-doped carbon nanospheres for efficient catalytic hydrogenation of Levulinic acid to c-valerolactone under solvent-free conditions. *J. Colloid Interface Sci.* **2022**, *623*, 905–914. [CrossRef] [PubMed]

85. Ding, D.; Wang, J.; Xi, J.; Liu, X.; Lu, G.; Wang, Y. High-yield production of levulinic acid from cellulose and its upgrading to γ-valerolactone. *Green Chem.* **2014**, *16*, 3846–3853. [CrossRef]